AD-A089 238 BROWN UNIV PROVIDENCE RI DEPT OF CHEMISTRY F/G 20/3
PHOTOELECTRONIC PROPERTIES OF TERNARY NIOBIUM OXIDES.(U)
SEP 80 K DWIGHT, A WOLD N00014-77-C-0387
UNCLASSIFIED TR-12 NL

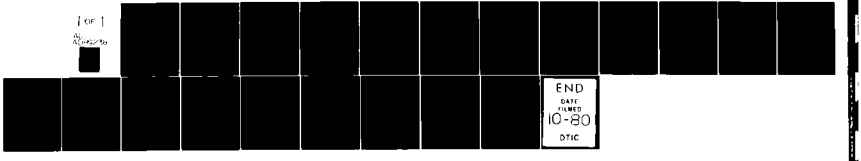

END
DATE FILMED
10-80
DTIC

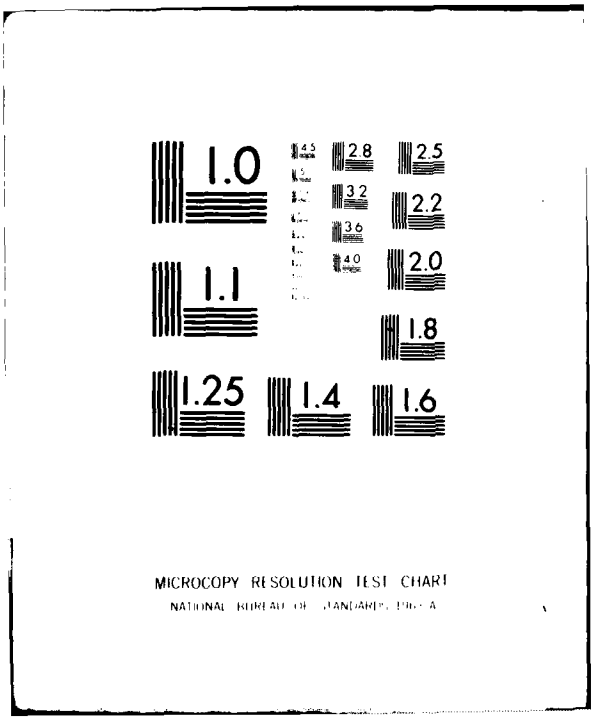
1.0
1.1
1.25
1.4
1.6
1.8
2.0
2.2
2.5
2.8
3.2
3.6
4.0
4.5
MICROCOPY RESOLUTION TEST CHART
NATIONAL BUREAU OF STANDARDS 1963-A

(12)

SECURITY CLASSIFICATION OF THIS PAGE (When Data Entered)

REPORT DOCUMENTATION PAGE	READ INSTRUCTIONS BEFORE COMPLETING FORM
1. REPORT NUMBER: 12	2. GOVT ACCESSION NO.: AD-A089 238	3. RECIPIENT'S CATALOG NUMBER
4. TITLE (and Subtitle): Photoelectronic Properties of Ternary Niobium Oxides	5. TYPE OF REPORT & PERIOD COVERED: (9) Technical
	6. PERFORMING ORG. REPORT NUMBER: 12
7. AUTHOR(s): (10) K. Dwight A. Wold	8. CONTRACT OR GRANT NUMBER(s): N000014-77-C-0387
9. PERFORMING ORGANIZATION NAME AND ADDRESS: Professor Aaron Wold, Brown University, Department of Chemistry, Providence, Rhode Island 02912	10. PROGRAM ELEMENT, PROJECT, TASK AREA & WORK UNIT NUMBERS: NR-359-653
11. CONTROLLING OFFICE NAME AND ADDRESS: Dr. David Nelson, Code 472, Office of Naval Research, Arlington, Virginia (11) Sep 80	12. REPORT DATE: September 1, 1980
	13. NUMBER OF PAGES: 20
14. MONITORING AGENCY NAME & ADDRESS (if different from Controlling Office): (14) TR-12	15. SECURITY CLASS. (of this report): LEVEL II
	15a. DECLASSIFICATION/DOWNGRADING SCHEDULE

16. DISTRIBUTION STATEMENT (of this Report)

Approved for Public Release; Distribution Unlimited

17. DISTRIBUTION STATEMENT (of the abstract entered in Block 20, if different from Report)

DTIC ELECTE SEP 17 1980 S D C

18. SUPPLEMENTARY NOTES

Submitted to ACS Symposium Series

19. KEY WORDS (Continue on reverse side if necessary and identify by block number)

ternary niobium oxides
photoelectronic properties
band gap
photoresponse
flat-band potential

20. ABSTRACT (Continue on reverse side if necessary and identify by block number)

A series of ternary niobium oxides were prepared and their photoelectronic properties evaluated. When two species of photoactive centers are simultaneously present, the higher flat-band potential appears to dominate. But it is evident that both species contribute their characteristic sets of inter-band transitions to the ensemble. In this respect, these oxide semiconductors behave differently than the conventional, broad-band semiconductors. It would appear that different photoactive centers remain at (over)

DD FORM 1 JAN 73 1473 EDITION OF 1 NOV 65 IS OBSOLETE S/N 0102-014-6601

405 736

SECURITY CLASSIFICATION OF THIS PAGE (When Data Entered)

20. Abstract (Continued)

least partially independent. Hence, for $FeNbO_4$, the data show all the characteristics of the (NbO_6^n) octahedra in addition to all the characteristics of the (FeO_6^n) centers.

OFFICE OF NAVAL RESEARCH

Contract N000014-77-C-0387

Task No. NR-359-653

TECHNICAL REPORT NO. 12

Photoelectronic Properties of Ternary Niobium Oxides

by

K. Dwight and A. Wold

Prepared for Publication

in the

ACS Symposium Series

Brown University

Department of Chemistry

Providence, Rhode Island

September 1, 1980

PHOTOELECTRONIC PROPERTIES OF TERNARY NIOBIUM OXIDES

K. Dwight and A. Wold
Department of Chemistry
Brown University
Providence, Rhode Island 02912

Ferric oxide is known to have an optical band gap of about 2 eV, and the literature contains many reports of photoelectrochemical measurements on "conducting", n-type Fe_2O_3 (1, 2, 3, 4, 5). Unfortunately, any attempt to reduce ferric oxide results in the formation of magnetite as a distinct separate phase, and there is no solubility of this spinel in the corundum structure (5, 6). Thus, all the properties reported above for Fe_2O_3 were measured either on multiphase samples or on samples which contained impurities.

The ternary iron oxides, as exemplified by the iron-niobium system, offer an opportunity to obtain single-phase, conducting n-type iron oxides; in which the conductivity can be controlled by means of chemical substitution. At first glance, $FeNbO_4$ and $FeNb_2O_6$ might appear to be very different materials. Yet as $MM'O_4$ and MM'_2O_6 they merely represent superstructures of the basic α-PbO_2 structure obtained under the conditions of preparation (7). Consequently, they form a solid solution in which the two valence states of iron are uniformly distributed throughout a single homogeneous phase (8).

However, many ternary systems incorporate a second photoactive center in addition to the $[FeO_6]$ octahedra: in the present case, $[NbO_6]$ octahedra. The interaction between such multiple centers has not previously been investigated. In the present work, interband transitions are observed which appear characteristic of niobium centers, together with other transitions characteristic of the iron centers. Since these are homogeneous, single-phase materials, this result suggests that caution should be exercised when applying the conventional band model to such oxide semiconductors.

For materials with a single photoactive center, it is generally observed that the optical band gap and flat-band potential are interrelated, so that lower band gaps appear to be accompanied by more positive flat-band potentials (4,9). Nevertheless, the non-active A-site ions in such ternary compounds as $BaTiO_3$, $SrTiO_3$, $Ba_{0.5}Sr_{0.5}Nb_2O_6$ and $Sr_2Nb_2O_7$ do have a perturbing effect

(4, 7, 9, 10). Consequently, it multiple photoactive centers can maintain sufficiently independent existence in a single compound, it would be conceivable that significant deviations from the usual correlation of high flat-band potentials with low band-gap energies might occur.

Effects of Composition and Structure

Before proceeding to ternary oxides with multiple photoactive centers, the effects of composition and structure upon such photoelectronic properties as optical band gap and flat-band potential for a given active center should be considered. It will be seen that composition appears to primarily affect the flat-band potential, whereas the band gap is more sensitive to structure.

$Sr_2Nb_2O_7$ is a pyrochlore; $Ba_{0.5}Sr_{0.5}Nb_2O_6$ is a defect perovskite. In both materials, the $[NbO_6]$ octahedra are the only photoactive centers. As shown in Figure 1, the flat-band potential of the pyrochlore is more negative by 0.4 volts, and its band gap is correspondingly larger, as would be expected. But the respective roles of structure and composition cannot be deduced from this comparison alone.

$BaTiO_3$ and $SrTiO_3$ are both perovskites and have nearly the same optical band gaps. Yet the flat-band potential of $SrTiO_3$ is 0.6 volts more negative than for the barium analog, a difference comparable in magnitude to that noted above for the niobates. Furthermore, it can be seen from Figure 1 that the band gap in the rutile TiO_2 is significantly lower than in these perovskite titanates.

Thus, the behavior in both the titanium and niobium systems is consistent with the hypothesis that the A-site cation is primarily responsible for variation in flat-band potential while the structure is primarily responsible for variation in optical band gap. Of course, it has been noted elsewhere that other properties such as the magnitude of the quantum efficiency also depend upon structure (10).

From Figure 1 it is evident that Fe_2O_3, $FeNbO_4$, and $FeTiO_3$ all have relatively positive flat-band potentials, which is presumably a characteristic of the iron. The band gap in the titanate appears to be associated with the $[TiO_6]$ octahedra; that in the niobate appears to match ferric oxide within structural variability. From such a cursory analysis, there would appear to be no effect from the presence of a second photoactive center in these two materials.

However, the existence of such an effect can be demonstrated by the application of a recently proposed technique for the study of interband transitions having energies greater than the "optical" band gap (11). Standard procedures exist for the extraction of band-gap information from measurement of the optical absorption coefficient, which has been shown to be proportional to the quantum efficiency (photocurrent density divided by the incident

light flux) under conditions applicable to the materials considered here (11, 12). The photoelectrolysis experiment provides an effective sampling region much thinner than can be obtained by polishing crystals, thereby extending the range of measurement to much higher energies. Since this technique is not yet widely known, an outline of its principal features is presented in the following section.

Band-Gap Analysis

Under moderate irradiation, the reaction rate in a photoelectrolysis cell is limited by the arrival rate of holes at the anode surface (12), in which case the quantum efficiency η is given by:

$$\eta = 1 - [\exp(-\alpha W)]/(1 + \alpha L_p)$$

where α is the optical absorption coefficient, L_p is the hole diffusion length, and W is the width of the depletion layer (12). Also,

$$W = [2\varepsilon\varepsilon_o (V-V_{fb})/eN_o]^{1/2}$$

and

$$L_p \leq [\varepsilon\varepsilon_o (kT/e)/eN_o]^{1/2}$$

since the hole diffusion length is determined by bulk recombination in highly defective oxides (11,12).

The dielectric constant ε can be estimated to be of the order of 100, and the donor concentration N_o can be estimated from the measured conductivity, activation energy and Hall mobility to be of the order of 10^{20} cm^{-3}. Then $W \simeq 10^{-6}$ cm and L_p is even smaller, so that expansion of the exponential yields a quantum efficiency proportional to the optical absorption coefficient even for large values of α.

The optical absorption coefficient for a single interband transition is related to the photon energy by $\alpha \sim (h\nu)^{-1}(h\nu - Eg)^n$ where Eg is the band gap and n depends upon the character of the transition (n = 0.5 for allowed direct transitions; n = 2 for allowed indirect ones). Thus, if experimental values for α are multiplied by $h\nu$ and are plotted as $(\alpha h\nu)^{(1/n}$ against $h\nu$, then a straight line intersecting the energy axis at Eg will be obtained when n correctly characterizes the transition. Since the total optical absorption coefficient α for a compound comprises the sum of such contributions from successive interband transitions, its complete analysis must proceed in stages. Each transition is characterized in turn, starting from the lowest energy, whereupon its contribution to the absorption is extrapolated to higher energies and subtracted from the total α. However, the simple determination of the interband transition energies does not require this elaborate process, the onset of each additional contribution

to the total α being clearly visible as an abrupt increase in the slope of the graph of $(\alpha h\nu)^{(1/n)}$ vs hν. Furthermore, higher-energy direct transitions can often be identified unambiguously without subtracting the contributions from lower-energy indirect ones.

The absorption coefficient increases with increasing photon energy, and each successive transition adds to the rate of increase. Consequently, the analysis of higher-energy transitions is limited by the maximum value of α which can be measured, which is inversely proportional to the thickness of the sample. In the photoelectrolysis experiment, the depletion layer forms a very narrow sampling region, so that the maximum value of α measurable by η is large. This permits the determination of interband transitions well above the energy of the lowest band gap (11).

In order to illustrate the power and reliability of this analytical procedure, the quantum efficiency η measured for $SrTiO_3$, being proportional to α, has been multiplied by the photon energy hν and is plotted in Figure 2 as $(\eta h\nu)^{0.5}$ vs hν. The linearity of the lowest-energy section of this graph (with n = 2) characterizes the transition as indirect. The energy intercept yields the value of 3.2 eV for the lowest band gap, which is in good agreement with previous absorption measurements (13) and with the calculation of Kahn and Leyendecker (14).

The abrupt increase in slope at 3.37 eV signals the presence of a higher-energy transition, in accord with the increased absorption found by electromodulation measurement (15). The decrease in slope at 3.5 eV corresponds to a saturation of this contribution to the total absorption and is not understood. Nevertheless, several other materials give evidence of similar behavior.

Finally, the transition at 3.74 eV agrees both with the electromodulation spectra (15) and with the band structure calculation (14). This higher-energy section does not appear greatly different from the rest of Figure 2, although there is some curvature of the data. However, this region becomes truly linear when replotted as $(\eta h\nu)^2$ versus hν, which establishes the direct character of the high-energy transition.

Results and Discussion

The quantum efficiency data for the defect pyrochlore $Ba_{0.5}Sr_{0.5}Nb_2O_6$ is presented in Figure 3 (10). It shows an indirect band gap at 3.4 eV with a "tail" extending to nearly 2.6 eV. The higher-energy transition at 4.4 eV shows some curvature of the data, and indeed, corresponds to a direct transition when replotted as $(\eta h\nu)^2$ versus energy (10).

Similar data for the pyrochlore $Sr_2Nb_2O_7$ is plotted in Figure 4. Here the principle indirect band gap occurs at 3.9 eV with a "tail" to nearly 3.4 eV. The data beyond 4.3 eV cannot be interpreted quantitatively because of a breakdown in the conditions required for the band-gap analysis, but there is an indication of

a transition in the vicinity of 4.7 eV. Thus the behavior is qualitatively similar to that observed in the perovskite niobate, only shifted to higher energies.

The analagous results for the corundum Fe_2O_3 are given in Figure 5. This shows an indirect band gap at 1.85 eV together with a direct band gap at 2.5 eV (11). Such simple behavior is in sharp contrast with the complex succession of transitions shown in Figure 6 for $FeNbO_4$ (7). Here the lowest-energy transition at 2.05 eV is clearly indirect. It is followed by several higher-energy transitions at 2.68, 2.93, 3.24, and 4.38 eV, each giving rise to a sudden increase in the slope of the curve, but so close together as to preclude reliable determination of direct or indirect character.

The locations of these additional interband transitions are highly suggestive. That at 2.68 eV appears to correlate with the 2.58 eV transition for Fe_2O_3 shown in Figure 5; those at 3.24, 2.9, and 4.38 eV are reminiscent of the indirect transition at 3.4 eV, its "tail," and the direct transition at 4.4 eV shown in Figure 3 for $Ba_{0.5}Sr_{0.5}Nb_2O_6$. Thus the data for $FeNbO_4$ show all the characteristics of the $[NbO_6]$ octahedra in addition to all the characteristics of the $[FeO_6]$ centers. The greater similarity to the perovskite niobate can be attributed to closer agreement between their Nb-O bond strengths as compared with those in the pyrochlore structure.

Summary and Conclusions

When only a single species of photoactive center is present in a compound, the presence of a non-active, A-site cation produces a characteristic shift in the flat-band potential. A change in structure, however, will in general produce a shift in the optical band-gap energy. This is accompanied by corresponding shifts in any other, higher-energy interband transition, but the qualitative features remain the same, and hence appear to be characteristic of the particular photoactive center.

When two species of photoactive centers are simultaneously present, the higher flat-band potential appears to dominate. But it is evident that both species contribute their characteristic sets of interband transitions to the ensemble. In this respect, these oxide semiconductors behave differently than the conventional, broad-band semiconductors. It would appear that different photoactive centers remain at least partially independent.

However, further experimentation embracing a variety of ternary systems will be required to determine the degree of interaction between such multiple centers. Preliminary results for Fe_2WO_6 confirm the superposition of two characteristic sets of interband transitions. The optical band gap and flat-band potential are essentially the same as in $FeNbO_4$, but the quantum efficiency is considerably greater. This suggests that there may be some enhancement of the photoresponse due to interaction between

the iron and tungsten centers.

Acknowledgements

The authors would like to acknowledge the support of the Office of Naval Research, Arlington, Virginia for the support of Kirby Dwight.

The authors would also like to acknowledge the Solar Energy Research Institute, Golden, Colorado as well as the Materials Research Laboratory Program at Brown University for their support.

Literature Cited

1. Hardee, K. L.; Bard, A. J. J. Electrochem. Soc., 1976, 123, 1024 and J. Electrochem. Soc., 1977, 124, 215.
2. Quinn, R. K.; Nasby, R. D.; Baughman, R. J. Mat. Res. Bull., 1976, 11, 1011.
3. Yeh, L. R.; Hackerman, N. J. Electrochem. Soc., 1977, 124, 833.
4. Kung, H. H.; Jarrett, H. S.; Sleight, A. W.; Ferretti, A. J. Appl. Phys., 1977, 48, 2463.
5. Merchant, P.; Collins, R.; Kershaw, R.; Dwight, K.; Wold, A. J. Solid State Chem., 1979, 27, 307.
6. Salmon, O. N. J. Phys. Chem., 1961, 65, 550.
7. Koenitzer, J.; Khazai, B.; Hormadaly, J.; Dwight, K.; Wold, A. J. Solid State Chem., to be published.
8. Turnock, A. C. J. of the Am. Ceramic Soc., 1966, 49, 177.
9. Nozik, A. J. Ann. Rev. Phys. Chem., 1978, 29, 189.
10. Hormadaly, J.; Subbarao, S. N.; Kershaw, R.; Dwight, K.; Wold, A. J. Solid State Chem., to be published.
11. Koffyberg, F. P.; Dwight, K.; Wold, A. Solid State Communications, 1979, 30, 433.
12. Butler, M. A. J. Appl. Phys., 1977, 48, 1914.
13. Weakliem, H. A.; Burk, W. J.; Redfield, D.; Korsum, V. R.C.A. Review, 1975, 36, 149.
14. Kahn, A. H.; Leyendecker, A. J. Phys. Rev., 1964, 135, A1321.
15. Mack, S. A.; Handler, P. Phys. Rev., 1974, B9, 3415.

Figure Captions

Figure 1 - Optical band gaps and flat-band potentials (adjusted to pH = 13) for some photoanode materials (4, 7, 9, 10).

Figure 2 - Band-gap analysis for $SrTiO_3$ (11), showing transitions at 3.2, 3.4, and 3.75 eV.

Figure 3 - Band-gap analysis for $Ba_{0.5}Sr_{0.5}Nb_2O_6$ (10), showing transitions at 2.6, 3.4, and 4.4 eV.

Figure 4 - Band-gap analysis for $Sr_2Nb_2O_7$ (10), showing transitions at 3.4 and 3.9 eV.

Figure 5 - Band-gap analysis for Fe_2O_3 (11), showing transitions at 1.85 and 2.58 eV.

Figure 6 - Band-gap analysis for $FeNbO_4$ (7), showing transitions at 2.05, 2.68, 2.9, 3.24, and 4.38 eV.

PHOTOELECTRONIC PROPERTIES

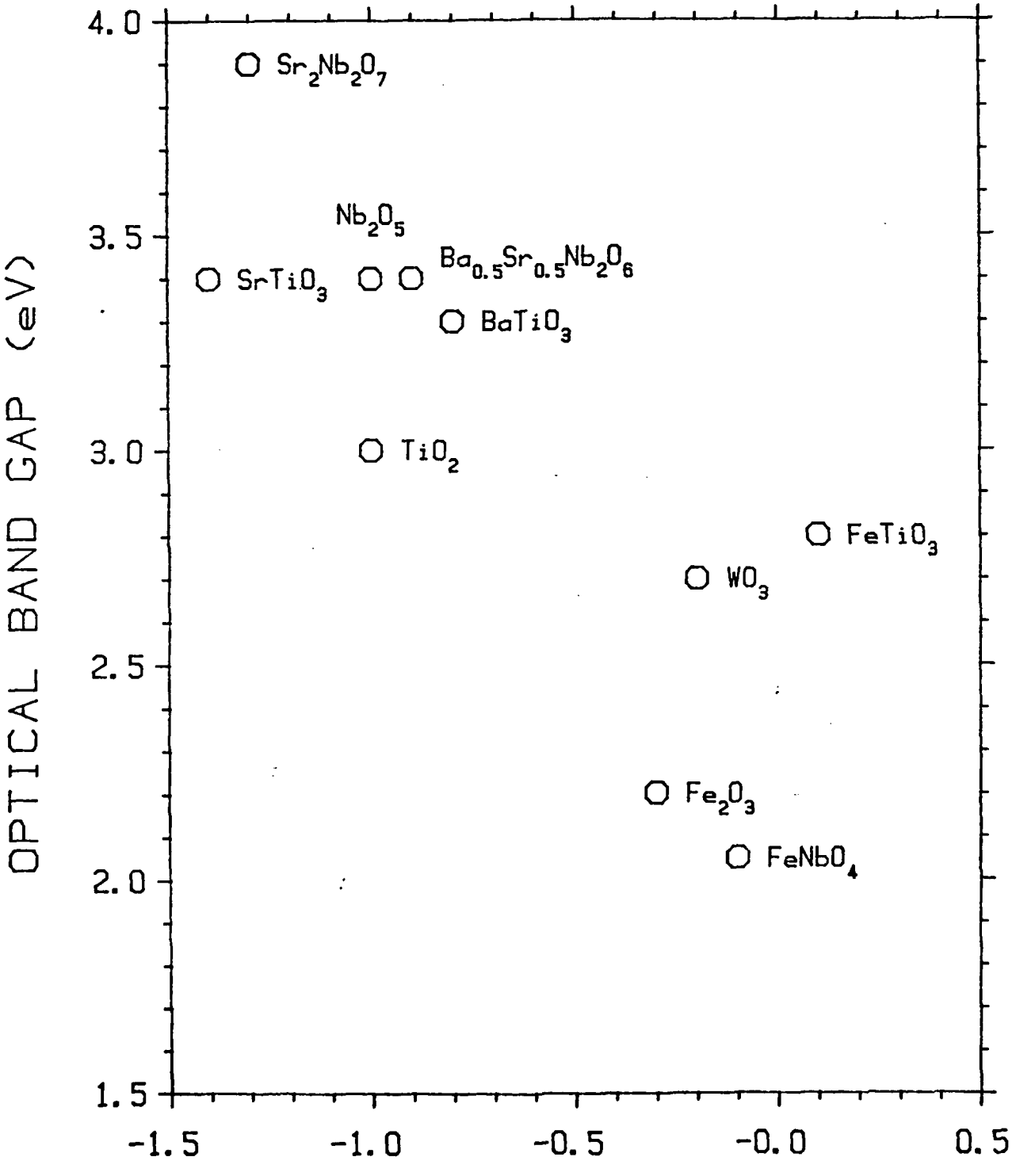

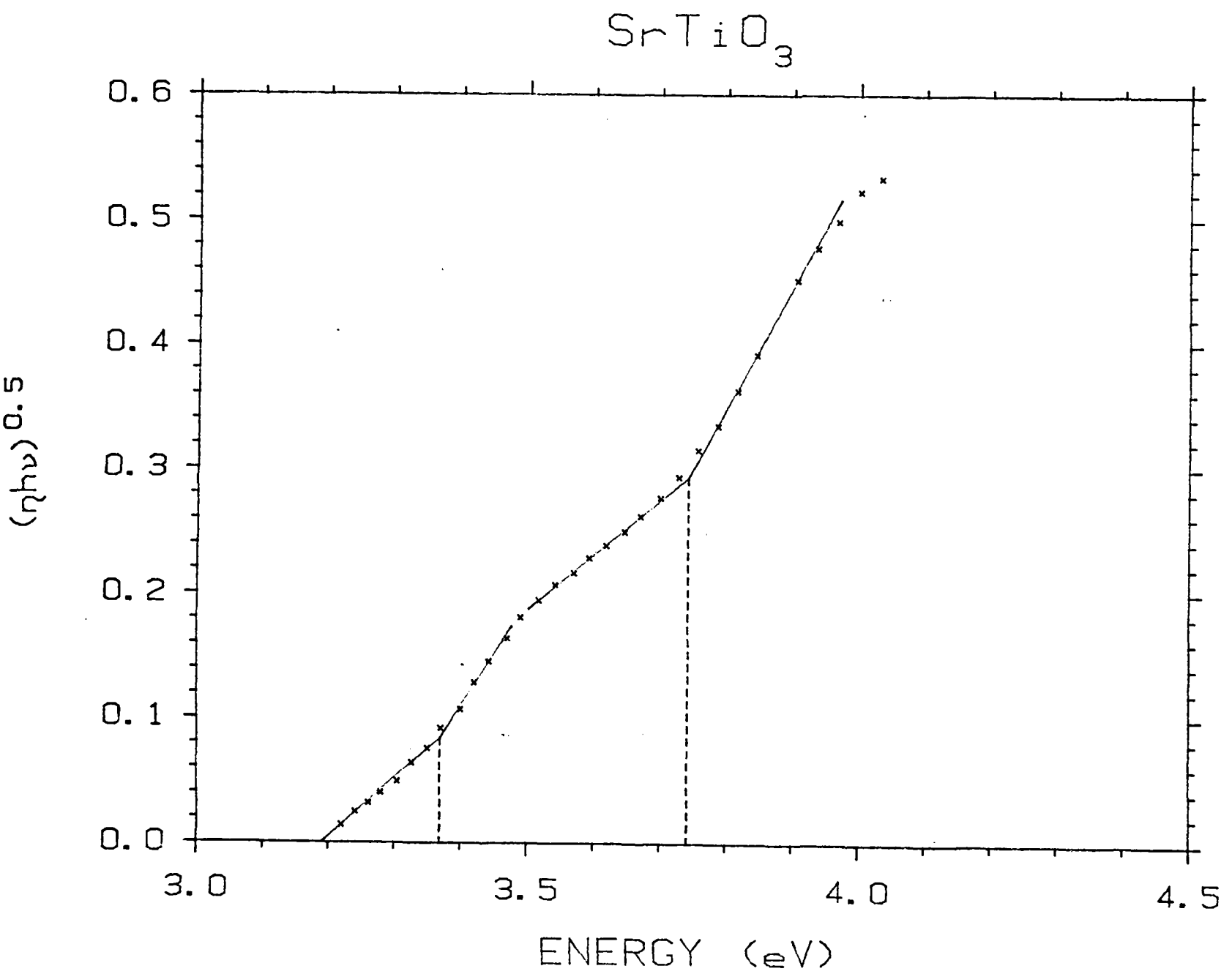
SrTiO3
0.6
0.5
0.4
0.3
0.2
0.1
0.0
(ηhν)0.5
3.0
3.5
4.0
4.5
ENERGY (eV)

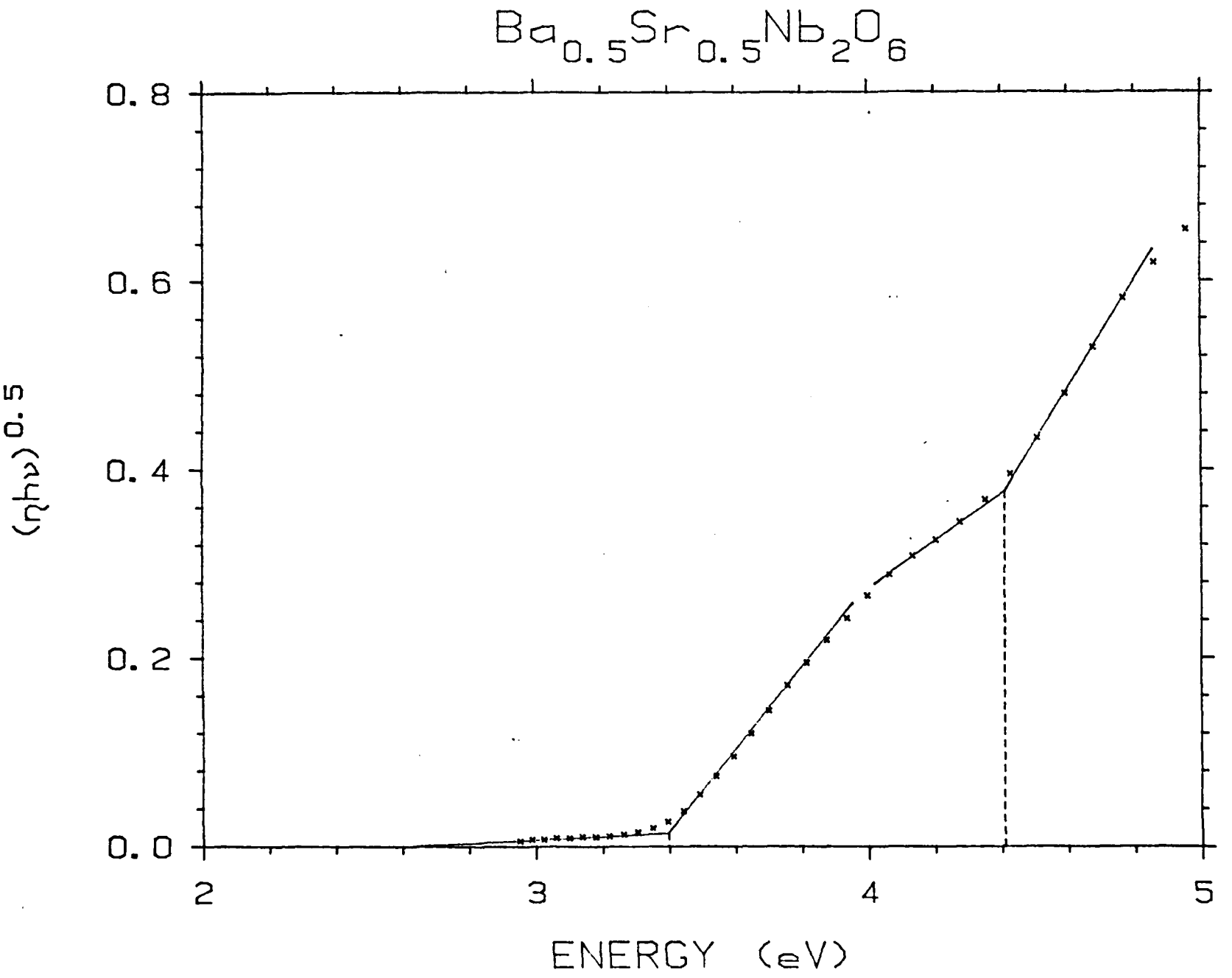
$Ba_{0.5}Sr_{0.5}Nb_2O_6$
0.8
0.6
0.4
0.2
0.0
$(\eta h\nu)^{0.5}$
2
3
4
5
ENERGY (eV)

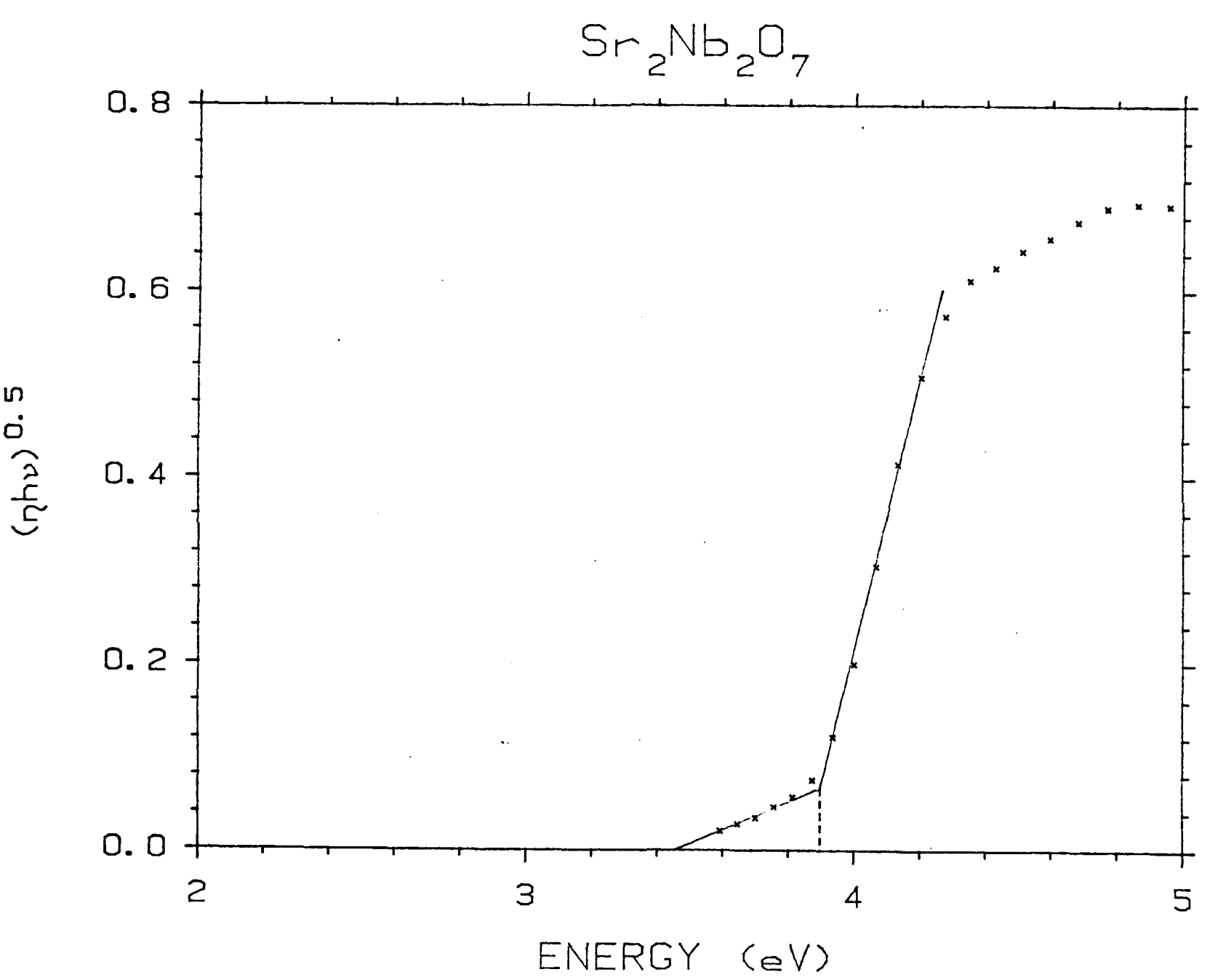
$Sr_2Nb_2O_7$
0.8
0.6
0.4
0.2
0.0
$(\eta h\nu)^{0.5}$
2
3
4
5
ENERGY (eV)

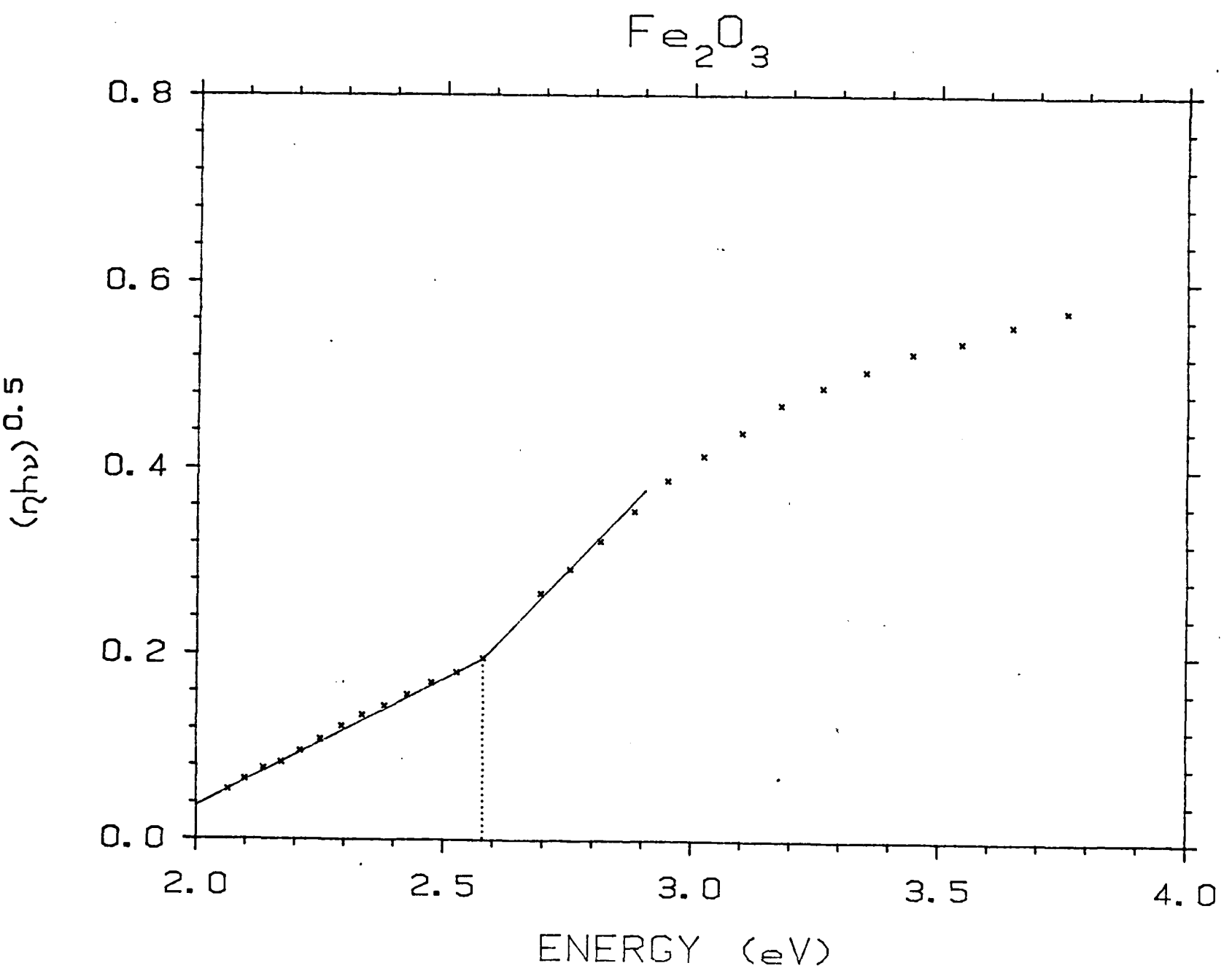
Fe_2O_3
0.8
0.6
0.4
0.2
0.0
$(\eta h\nu)^{0.5}$
2.0
2.5
3.0
3.5
4.0
ENERGY (eV)

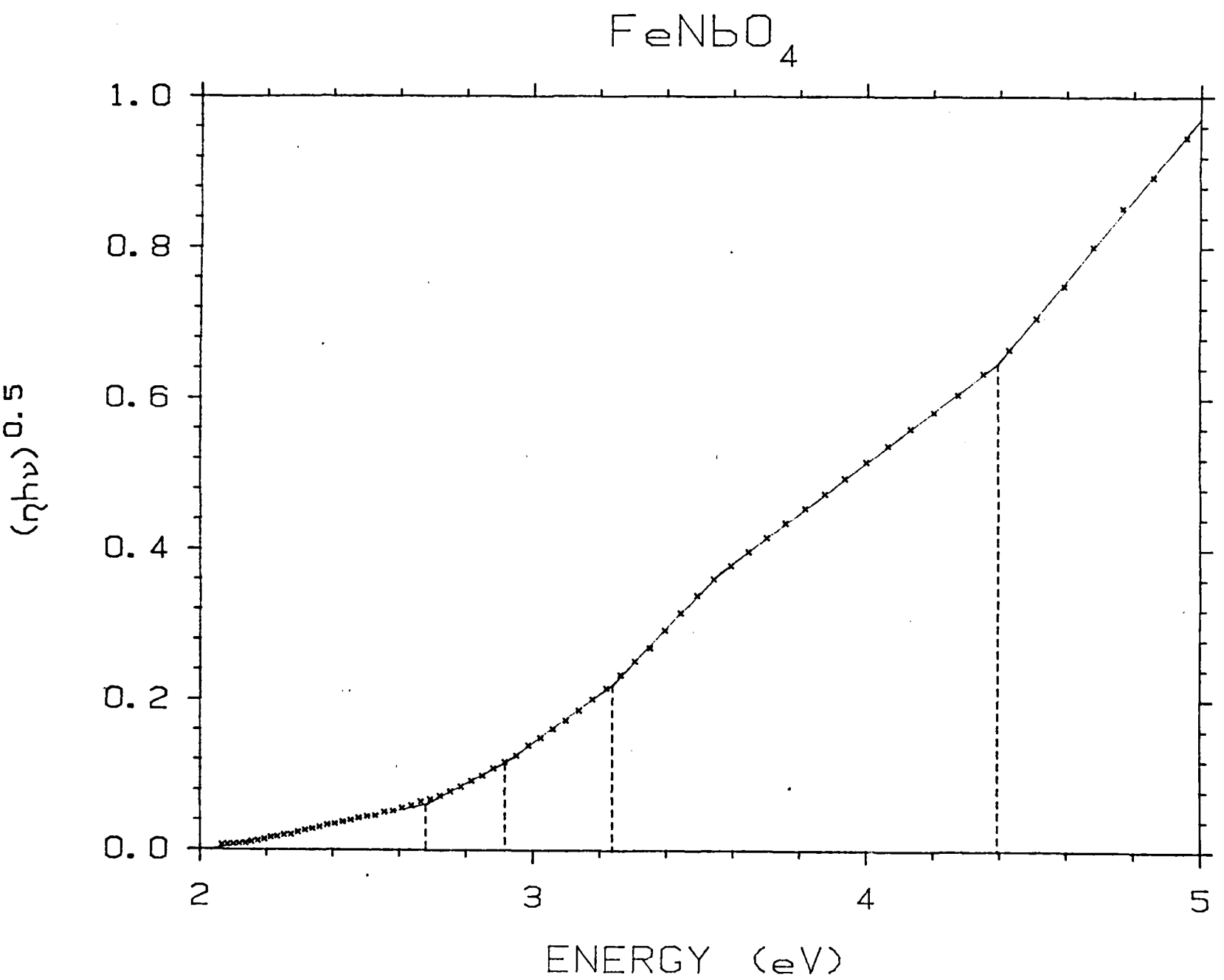
FeNbO4
1.0
0.8
0.6
0.4
0.2
0.0
(ηhν)0.5
2
3
4
5
ENERGY (eV)

TECHNICAL REPORT DISTRIBUTION LIST, GEN

	No. Copies
Office of Naval Research Attn: Code 472 800 North Quincy Street Arlington, Virginia 22217	2
ONR Branch Office Attn: Dr. George Sandoz 536 S. Clark Street Chicago, Illinois 60605	1
ONR Area Office Attn: Scientific Dept. 715 Broadway New York, New York 10003	1
ONR Western Regional Office 1030 East Green Street Pasadena, California 91106	1
ONR Eastern/Central Regional Office Attn: Dr. L. H. Peebles Building 114, Section D 666 Summer Street Boston, Massachusetts 02210	1
Director, Naval Research Laboratory Attn: Code 6100 Washington, D.C. 20390	1
The Assistant Secretary of the Navy (RE&S) Department of the Navy Room 4E736, Pentagon Washington, D.C. 20350	1
Commander, Naval Air Systems Command Attn: Code 310C (H. Rosenwasser) Department of the Navy Washington, D.C. 20360	1
Defense Technical Information Center Building 5, Cameron Station Alexandria, Virginia 22314	12
Dr. Fred Saalfeld Chemistry Division, Code 6100 Naval Research Laboratory Washington, D.C. 20375	1
U.S. Army Research Office Attn: CRD-AA-IP P.O. Box 1211 Research Triangle Park, N.C. 27709	1
Naval Ocean Systems Center Attn: Mr. Joe McCartney San Diego, California 92152	1
Naval Weapons Center Attn: Dr. A. B. Amster, Chemistry Division China Lake, California 93555	1
Naval Civil Engineering Laboratory Attn: Dr. R. W. Drisko Port Hueneme, California 93401	1
Department of Physics & Chemistry Naval Postgraduate School Monterey, California 93940	1
Dr. A. L. Slafkosky Scientific Advisor Commandant of the Marine Corps (Code RD-1) Washington, D.C. 20380	1
Office of Naval Research Attn: Dr. Richard S. Miller 800 N. Quincy Street Arlington, Virginia 22217	1
Naval Ship Research and Development Center Attn: Dr. G. Bosmajian, Applied Chemistry Division Annapolis, Maryland 21401	1
Naval Ocean Systems Center Attn: Dr. S. Yamamoto, Marine Sciences Division San Diego, California 91232	1
Mr. John Boyle Materials Branch Naval Ship Engineering Center Philadelphia, Pennsylvania 19112	1

TECHNICAL REPORT DISTRIBUTION LIST, GEN

	No. Copies
Dr. Rudolph J. Marcus Office of Naval Research Scientific Liaison Group American Embassy APO San Francisco 96503	1
Mr. James Kelley DTNSRDC Code 2803 Annapolis, Maryland 21402	1

TECHNICAL REPORT DISTRIBUTION LIST, 359

	No. Copies
Dr. Paul Delahay Department of Chemistry New York University New York, New York 10003	1
Dr. E. Yeager Department of Chemistry Case Western Reserve University Cleveland, Ohio 41106	1
Dr. D. N. Bennion Department of Chemical Engineering Brigham Young University Provo, Utah 84602	1
Dr. R. A. Marcus Department of Chemistry California Institute of Technology Pasadena, California 91125	1
Dr. J. J. Auborn Bell Laboratories Murray Hill, New Jersey 07974	1
Dr. Adam Heller Bell Laboratories Murray Hill, New Jersey 07974	1
Dr. T. Katan Lockheed Missiles & Space Co, Inc. P.O. Box 504 Sunnyvale, California 94088	1
Dr. Joseph Singer, Code 302-1 NASA-Lewis 21000 Brookpark Road Cleveland, Ohio 44135	1
Dr. B. Brummer EIC Incorporated 55 Chapel Street Newton, Massachusetts 02158	1
Library P. R. Mallory and Company, Inc. Northwest Industrial Park Burlington, Massachusetts 01803	1
Dr. P. J. Hendra Department of Chemistry University of Southhampton Southhampton SO9 5NH United Kingdom	1
Dr. Sam Perone Department of Chemistry Purdue University West Lafayette, Indiana 47907	1
Dr. Royce W. Murray Department of Chemistry University of North Carolina Chapel Hill, North Carolina 27514	1
Naval Ocean Systems Center Attn: Technical Library San Diego, California 92152	1
Dr. C. E. Mueller The Electrochemistry Branch Materials Division, Research & Technology Department Naval Surface Weapons Center White Oak Laboratory Silver Spring, Maryland 20910	1
Dr. G. Goodman Globe-Union Incorporated 5757 North Green Bay Avenue Milwaukee, Wisconsin 53201	1
Dr. J. Boechler Electrochimica Corporation Attention: Technical Library 2485 Charleston Road Mountain View, California 94040	1
Dr. P. P. Schmidt Department of Chemistry Oakland University Rochester, Michigan 48063	1
Dr. H. Richtol Chemistry Department Rensselaer Polytechnic Institute Troy, New York 12181	1

TECHNICAL REPORT DISTRIBUTION LIST, 359

	No. Copies
Dr. A. B. Ellis Chemistry Department University of Wisconsin Madison, Wisconsin 53706	1
Dr. M. Wrighton Chemistry Department Massachusetts Institute of Technology Cambridge, Massachusetts 02139	1
Larry E. Plew Naval Weapons Support Center Code 30736, Building 2906 Crane, Indiana 47522	1
S. Ruby DOE (STOR) 600 E Street Washington, D.C. 20545	1
Dr. Aaron Wold Brown University Department of Chemistry Providence, Rhode Island 02192	1
Dr. R. C. Chudacek McGraw-Edison Company Edison Battery Division Post Office Box 28 Bloomfield, New Jersey 07003	1
Dr. A. J. Bard University of Texas Department of Chemistry Austin, Texas 78712	1
Dr. M. M. Nicholson Electronics Research Center Rockwell International 3370 Miraloma Avenue Anaheim, California	1
Dr. Donald W. Ernst Naval Surface Weapons Center Code R-33 White Oak Laboratory Silver Spring, Maryland 20910	1
Dr. R. P. Van Duyne Department of Chemistry Northwestern University Evanston, Illinois 60201	1
Dr. B. Stanley Pons Department of Chemistry University of Alberta Edmonton, Alberta CANADA T6G 2G2	1
Dr. Michael J. Weaver Department of Chemistry Michigan State University East Lansing, Michigan 48824	1
Dr. R. David Rauh EIC Corporation 55 Chapel Street Newton, Massachusetts 02158	1
Dr. J. David Margerum Research Laboratories Division Hughes Aircraft Company 3011 Malibu Canyon Road Malibu, California 90265	1
Dr. Martin Fleischmann Department of Chemistry University of Southampton Southampton SO9 5NH England	1
Dr. Janet Osteryoung Department of Chemistry State University of New York at Buffalo Buffalo, New York 14214	1
Dr. R. A. Osteryoung Department of Chemistry State University of New York at Buffalo Buffalo, New York 14214	1
Mr. James R. Moden Naval Underwater Systems Center Code 3632 Newport, Rhode Island 02840	1

TECHNICAL REPORT DISTRIBUTION LIST, 359

	No. Copies
Dr. R. Nowak Naval Research Laboratory Code 6130 Washington, D.C. 20375	1
Dr. John F. Houlihan Shenango Valley Campus Pennsylvania State University Sharon, Pennsylvania 16146	1
Dr. M. G. Sceats Department of Chemistry University of Rochester Rochester, New York 14627	1
Dr. D. F. Shriver Department of Chemistry Northwestern University Evanston, Illinois 60201	1
Dr. D. H. Whitmore Department of Materials Science Northwestern University Evanston, Illinois 60201	1
Dr. Alan Bewick Department of Chemistry The University Southampton, S09 5NH England	1
Dr. A. Himy NAVSEA-5433 NC #4 2541 Jefferson Davis Highway Arlington, Virginia 20362	1
Dr. John Kincaid Department of the Navy Stategic Systems Project Office Room 901 Washington, DC 20376	1
M. L. Robertson Manager, Electrochemical Power Sonices Division Naval Weapons Support Center Crane, Indiana 47522	1
Dr. Elton Cairns Energy & Environment Division Lawrence Berkeley Laboratory University of California Berkeley, California 94720	1
Dr. Bernard Spielvogel U.S. Army Research Office P.O. Box 12211 Research Triangle Park, NC 27709	1
Dr. Denton Elliott Air Force Office of Scientific Research Bldg. 104 Bolling AFB Washington, DC 20332	1

END

DATE
FILMED
10-80

DTIC